Science Education Technology Publisher

Published by SET Publisher

Journal of Basic & Applied Sciences

ISSN (online): 1927-5129

Calculation of the Relaxation Time and the Activation Energy Close to the Lower Phase Transition in Imidazolium Perchlorate

N. Kara[1,2], A. Kiraci[3] and Hamit Yurtseven[2,*]

[1]*Graduate School of Natural and Applied Sciences, Cankaya University, Ankara 06530, Turkey*

[2]*Department of Physics, Middle East Technical University, Ankara 06531, Turkey*

[3]*Inter-Curricular Courses Department, Cankaya University, Ankara 06790, Turkey*

Article Info:

Keywords:
Phase transition,
Ising model,
relaxation time,
activation energy,
imidazolium perchlorate.

Timeline:
Received: July 10, 2021
Accepted: August 01, 2021
Published: August 11, 2021

Citation: Kara N, Kiraci A, Yurtseven H. Calculation of the relaxation time and the activation energy close to the lower phase transition in imidazolium perchlorate. J Basic Appl Sci 2021; 17: 79-86.

DOI: https://doi.org/10.29169/1927-5129.2021.17.09

Abstract:

The temperature dependence of the relaxation time of imidazolium perchlorate (Im-ClO_4) was calculated from the pseudospin-phonon coupled (PS) and the energy fluctuation (EF) models close to the first-order phase transition temperature of 247 K. This calculation was performed in terms of the proton second moment M_2 that was associated with the order parameter which was predicted from the mean-field theory. Our results were in good agreement with the observed data. In addition, values of the activation energy were deduced in terms of the Arrhenius plot using our calculated values of the relaxation time from both PS and EF models.

*Corresponding Author
E-mail: hamit@metu.edu.tr

INTRODUCTION

Imidazolium salts (IMSs) are derivatives of imidazole rings that are ubiquitous and can bond to metals as a ligand and to form hydrogen bonds with drugs and proteins [1]. Differently from their parent's imidazoles, IMSs can interact electrostatically with biological systems since they lose the ability to bond both metals and hydrogen [2]. Imidazolium salts are known as room temperature ionic liquids (RTILs) consisting of large organic cations and inorganic anions that can be used as electrolytes as they have wide chemical stability [3] and unusual catalytic properties [4,5]. They are also used to extract metal ions from aqueous solutions and coat metal nanoparticles [6], dissolve carbohydrates [7], and create polyelectrolyte brushes on surfaces [8]. Organic-inorganic molecular ferroelectrics have come to prominence in comparison to the ferroelectric oxides since their advantageous characteristics, namely being environment-friendly (especially lead-free structure), having both low-cost and mechanically flexible structure [9,10]. In particular, as a member of organic-inorganic molecular ferroelectrics, imidazolium perchlorate ($C_3N_2H_5ClO_4$ or Im-ClO_4) can be used as an effective 3D printed metamaterial that produces rapid-prototype for reducing the manufacturing time of ferroelectrics from hours to minutes, as pointed out previously [11]. In addition, the thin film of Im-ClO_4 is reported [12] to exhibit superior electromechanical coupling exceeding that of PZT films, making them an attractive lead-free alternative for a variety of applications in sensor technology and electro-optics.

The performance of a system is significant in the field of solar energy for sustainable development. Organic-inorganic hybrid metal-halide perovskite solar cells (PSCs) are considered the next-generation photovoltaic technology. However, surface defects have been a major limitation for perovskite photovoltaics. Imidazolium-based ionic liquids have been reported [13] to be an excellent candidate for surface passivation and for reducing the energy barrier between the perovskite and hole transport layer (higher electron mobility) leading to high-efficiency perovskite solar cells.

Im-ClO_4 has been reported [14] to undergo three successive solid-solid phase transitions, namely, at 487, 373, and 247 K. The crystal structure of Im-ClO_4 is given [14] to be trigonal at room temperature with a space group R3m, Z=1, and the lattice parameter a = 5.484(1) $\AA$ with α = 95.18(2)°. Also, cations are strongly disordered where the perchlorate ions are ordered at room temperature, as reported earlier [14]. Above the room temperature, the crystal structure is also trigonal with a space group R$\bar{3}$m, a = 5.554(1) $\AA$ and α = 95.30(2)°, however all ionic sublattices are disordered [14]. The dielectric and optical properties of Im-ClO_4 have been declared by Czapla *et al.* [15] by studying the x-ray diffraction, dielectric, and birefringence measurements. The precise measurements of the specific heat changes of this crystal have been performed by Przeslawski and Czapla [16] using an ac calorimeter. The polymorphic phase transitions, the appearance of the ferroelectricity, molecular structure, and molecular dynamics of Im-ClO_4 have been investigated by Pajak *et. al.* [14] using differential scanning calorimetry (DSC), proton NMR relaxation, and the second moment, x-ray diffraction and dielectric spectroscopy measurements.

In the present study, the proton spin-lattice relaxation time (SLRT), denoted as T_1 (s) has been calculated as a function of temperature in the vicinity of the solid-solid phase transition temperature (T_C = 247 K), by using both the pseudospin-phonon (PS) coupled and the energy fluctuation (EF) models. This calculation has been performed by using the observed [14] proton second moment (M_2) as an order parameter below T_C and as a disorder parameter above T_C according to both models. Moreover, the fitting procedure was implemented for the calculated data of SLRT, by obtaining the fitting parameters at first, then the attitude of the observed values of SLRT was denoted around the transition temperature. Finally, the activation energy values were computed from the correlation of the damping constant concerning the reciprocal of temperature. We used these two models (PS and EF) in our previous studies to calculate some thermodynamic quantities such as the damping constant, frequency, relaxation time and the activation energy for $Cd_2Nb_2O_7$ [17], $BaTiO_3$[18,19], $PbTiO_3$ [20], KH_2PO_4 [21], PZT [22], $SrZrO_3$ [23], and very recently for $SrTiO_3$ [24] and $LiTaO_3$ [25].

Below, "Theory" was given in section 2. In section 3, the "Calculation and results" were given. The "Discussion" and "Conclusions" parts were given in sections 4 and 5, respectively.

2. THEORY

The damping constant $\Gamma_{sp}(\vec{k}\nu, \omega_\nu)$ due to the pseudospin-phonon interaction is given by the imaginary part of the self-energy which reads as [26]

$$\Gamma_{sp}(\vec{k}\nu,\omega_\nu) \simeq A\int_{BZ} S(\vec{q},\omega)\left[\frac{n(\omega_\nu)}{n(\omega)+1}+1\right]d^3q + B \quad \#(2.1)$$

In Eq. (2.1) the integral is taken over all the wavevector q in the Brillouin Zone (BZ). A and B are constants, $\vec{k}$ is the wavevector of the ν^{th} phonon, ω_ν is the peak frequency and S is the dynamic scattering function of the pseudospins that describes the anomalous behavior of the damping constant close to the transition temperature (T_C) according to [27]

$$S(q,\omega) = \langle n(\omega)+1\rangle \frac{\chi(q,0)\omega\tau_q}{1+(\omega\tau_q)^2} \quad \#(2.2)$$

where χ is the dielectric susceptibility, τ_q is the relaxation time of the order parameter with the wavevector q. Eq. (2.2) can be expressed as follows (Eq. 2.3) by using the approximations $n(\omega)+1 = (kT/\hbar\omega)$, $(\omega\tau_q)^2 \ll 1$ and $n(\omega_\nu)/[n(\omega)+1] \ll 1$ for $\omega \simeq 0$,

$$\Gamma_{sp} \approx \frac{AkT}{\hbar}\int_{BZ} \chi(q,0)\tau_q\, d^3q + B \quad \#(2.3)$$

In their study, Laulicht and Luknar [26] have reported the following expression using the random phase approximation which reads as

$$\chi(q,0)\tau_q = \frac{C\,(1-P^2)}{T}\frac{\tau_q^2}{\tau} \quad \#(2.4)$$

Here C is the Curie constant, P is the fractional spontaneous polarization (order parameter), τ is the proton flipping time. Lahajnar *et. al.* [28] have calculated the integration of Eq. (2.3) using Eq. (2.4) for KDP crystal given by

$$\Gamma_{sp} \propto \frac{1}{T_1} \propto (1-P^2)ln\left[\frac{T_C}{T-T_C(1-P^2)}\right] \quad \#(2.5)$$

where T_1 represents the proton spin-lattice relaxation time. Eq (2.5) defines the temperature dependence of the damping constant (or relaxation time) for the pseudospin-phonon coupled (PS) model. On the other hand, the damping constant (relaxation time) is related to the fluctuation of the frequencies at zero wavevectors [29] given by

$$\Gamma_{sp}^2 \propto \frac{kT\chi(0)}{V} \quad \#(2.6)$$

where V is the volume of the crystal. Schaack and Winterfeldt [29] have reported the following expression for the damping constant by inserting Eq. (2.4) in Eq. (2.6) that reads as

$$\Gamma_{sp} \propto \frac{1}{T_1} \propto \left(\frac{T(1-P^2)}{T-T_C(1-P^2)}\right)^{\frac{1}{2}} \quad \#(2.7)$$

So, that Eq. (2.7) defines the critical broadening of the damping constant due to the energy fluctuation (EF model).

3. CALCULATIONS AND RESULTS

The temperature dependence of the spin-lattice relaxation time (τ_1) for the Im-ClO$_4$ crystal has been calculated from the pseudospin-phonon (PS) coupled (Eq.2.5) and the energy fluctuation (EF) model (Eq 2.7) in the vicinity of the phase transition temperature of $T_C = 247\,K$. For this calculation, the observed [14] proton second moment (M_2) has been associated with the order parameter (P) and the disorder parameter ($1-P^2$) below and above T_C, respectively. Our calculated τ_{cal} from both models (PS and EF) were then fitted to the observed data τ_{obs} [14] according to

$$1/\tau_{obs} = b_0 + b_1(1/\tau)_{calc} + b_2(1/\tau)^2_{calc} \#(3.1)$$

Our calculated (Eqs. 2.5 and 2.7) values of τ_1 were fitted to the measured data [14], as given in Figure **1**. The fitting parameters b_0, $b_1$and b_2 were tabulated in Table **1**. Figure **2** gives our calculated (Eqs. 2.5 and 2.7) and measured data [14] of the spin-lattice relaxation time as a function of temperature. The activation energy U can also be calculated from the SLRT according to [30]

$$\ln(1/\tau) = \ln C - U/k_BT \quad \#(3.2)$$

Our calculated τ^{-1} from both PS (Eq 2.5) and EF (Eq 2.7) models were plotted as a function of T^{-1} according to Eq. (3.2) as given in Figure **3**. The activation energy U and the constant C were then extracted below and above T_C for Im-ClO$_4$, as given in Table **2**.

4. DISCUSSION

Im-ClO$_4$ exhibits three successive phase transitions as the temperature at 487, 373, and 247 K, as indicated previously. In the present study, we considered particularly the lower phase transition (T_C= 247 K) to explain the mechanism of the first-order transition since the inverse spin relaxation time (τ_1^{-1}) shows anomalous transition at T_C (Figure **2**), as observed experimentally

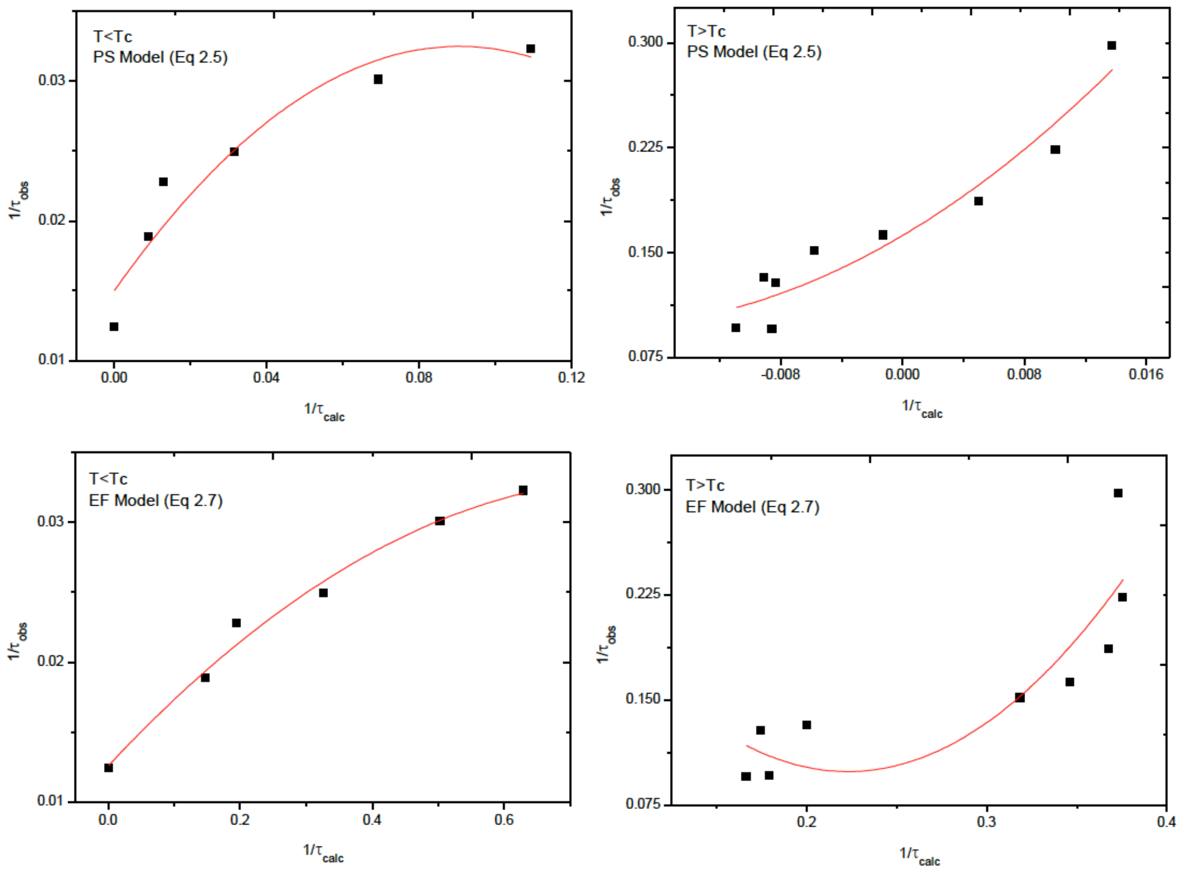

Figure 1: The inverse spin lattice relaxation for the experimental [14] and calculated (Eqs. 2.5 and 2.7) at various temperatures. The solid curves represent the best fit to the experimental data.

Table 1: Values of the Coefficients b_0, b_1 and b_2 according to Eq. (3.1) below and above the Transition Temperature (T_C= 247 K) of Im-ClO_4

Crystal	Model	b_0 x 10^{-2} (s^{-1})	b_1 x 10^{-2}	b_2 x 10^{-2} (s^{-1})	Temperature Interval
$ImClO_4$	PS (Eq. 2.5)	1.5	38.6	-213.3	142.9 < T (K) < 236.0
	PS (Eq. 2.5)	16.2	644.7	15776.0	251.0 < T (K) < 357.4
	EF (Eq. 2.7)	1.3	5.1	-3.1	142.9 < T (K) < 236.0
	EF (Eq. 2.7)	39.0	-261.6	587.3	251.0 < T (K) < 357.4

[14]. This is accompanied by the proton second moment (M_2) as an order parameter, which also shows discontinuous behavior at T_C (Figure **4**), as observed experimentally. These are the basic criteria we used to describe the lower phase transition (T= 247 K) in Im-ClO_4

Although it is difficult to explain the physical mechanism without knowledge of the low-temperature crystal structure of Im-ClO_4, the proton second moment M_2 below T_C = 247 K can be considered as an order parameter P, as pointed out previously for pyridinium periodate [31] and pyridinium flurosulfonate [32]. The molecular field theory provides the temperature dependence of the order parameter P below the phase transition given as

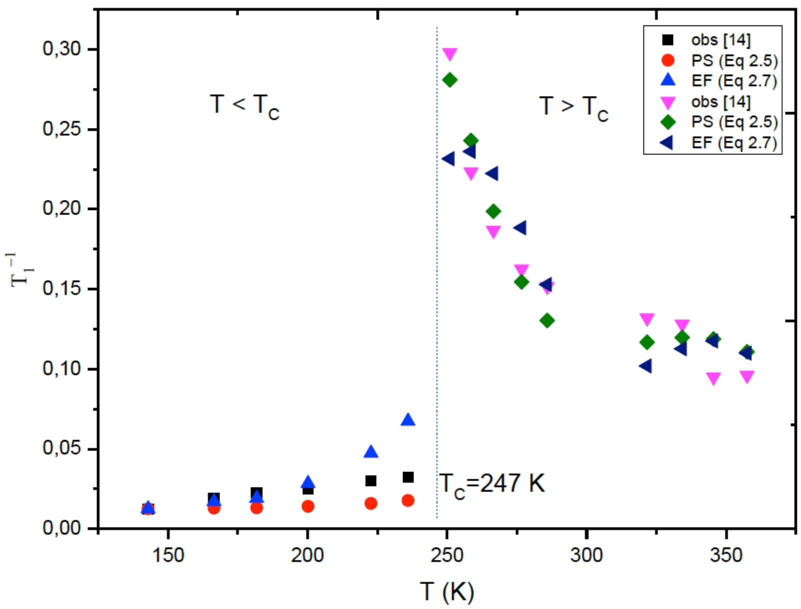

Figure 2: The temperature dependence of the spin lattice relaxation time T_1 calculated from the PS and EF models both below and above the solid-solid phase transition temperature of T_C = 247 K in $ImClO_4$.

Table 2: Values of the Activation Energy U and the Constant C according to Eq. (3.2) for the Cation Reorientation in Im-ClO_4

Crystal	Model	$U(kJ/mol)$	C x 10^{-3} (s^{-1})	Temperature Interval
$ImClO_4$	PS (Eq. 2.5)	2.4	107.7	142.9 < T (K) < 236.0
	PS (Eq. 2.5)	13.5	0.4	251.0 < T (K) < 285.9
	EF (Eq. 2.7)	4.9	650.9	142.9 < T (K) < 236.0
	EF (Eq. 2.7)	9.8	2.5	251.0 < T (K) < 285.9

$$P \approx \begin{cases} 1-\exp\left(\frac{-2T_C}{T}\right) & T \ll T_C \\ \left\{3\left(1-\frac{T}{T_C}\right)\right\}^{\frac{1}{2}} & 0 < (T_C - T) < T_C \\ 0 & T_C < T \end{cases} \#(4.1)$$

For the lower phase transition (T_C= 247 K) in Im-ClO_4 we considered the proton second moment (M_2) as an order parameter as stated above, about the spontaneous polarization (P) according to

$$M_2/M_{2max} = a_0 + a_1 P \#(4.2)$$

which was used in the PS (Eq. 2.4) and EF (Eq. 2.7) models. Since the spontaneous polarization (P) was used as an order parameter for both models (PS and EF) to study the phase transitions in the KDP type crystals [26-28], the temperature dependence of the proton second moment (M_2) was then considered to govern the mechanism of the order-disorder transition at T= 247 K in Im-ClO_4. The temperature dependence of M_2 is defined as an order parameter below T_C, $1 - M_2/M_{2max}$ (normalized) as a disorder parameter above T_C, were calculated from the molecular field theory (Eq. 4.1). Thus, in analogy with the M_2, the temperature dependence of the spontaneous polarization was the preliminary parameter in our treatment given here.

By fitting the order parameter from the mean-field theory (Eq. 4.1) to the experimental M_2/M_{2max} data [14] for Im-ClO_4, the coefficients a_0 and a_1 were determined as given in Table **3**. Figure **3** gives our calculated (Eq. 4.2) proton second moment M_2 normalized concerning the order parameter as a function of temperature for Im-ClO_4. The experimental data [14] were also given in

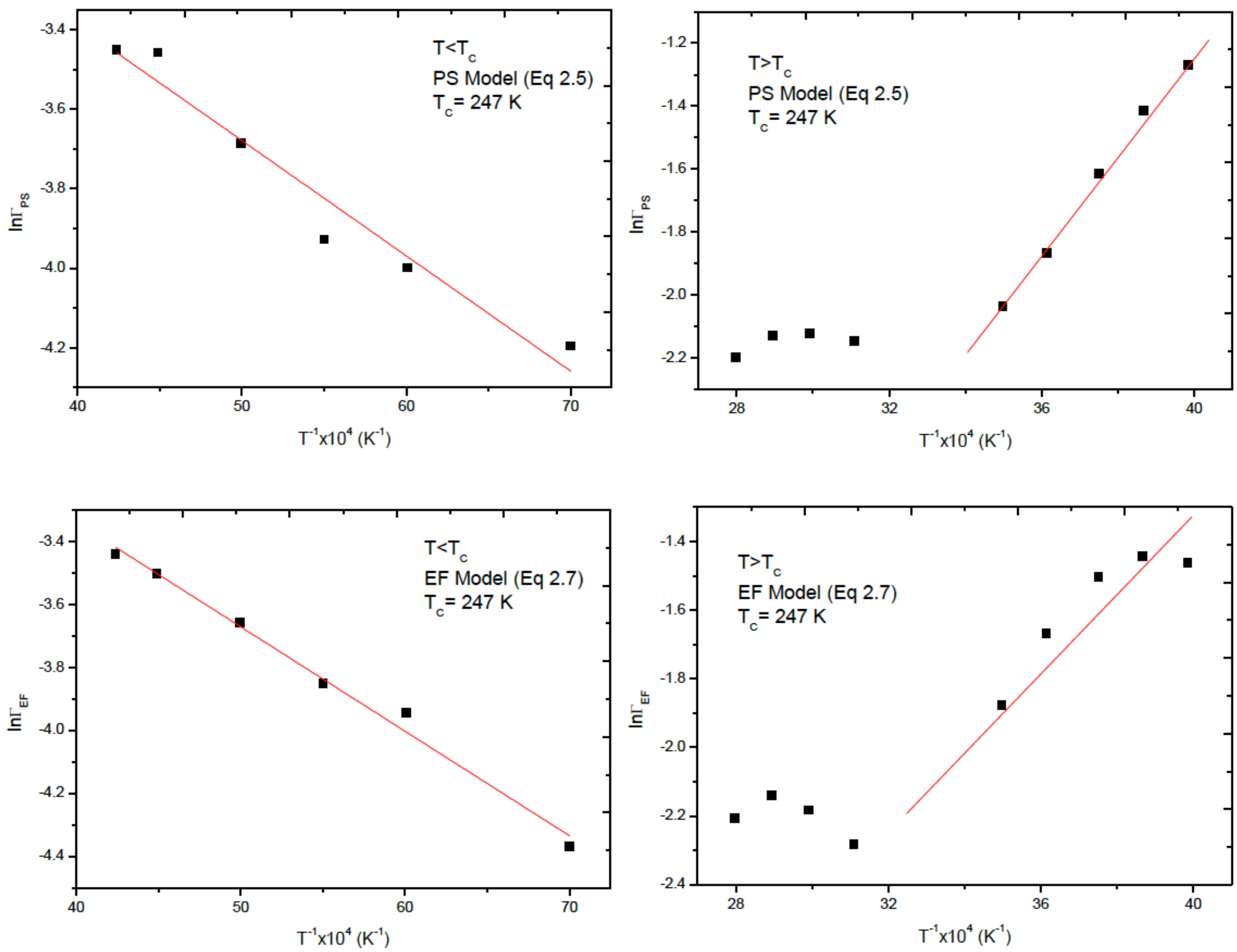

Figure 3: The damping constant Γ_{SP} calculated from Eqs. 2.5 (PS) and Eqs. 2.7 (EF) as a function of the reciprocal temperature to extract the activation energy for the cation reorientation in $ImClO_4$.

Table 3: Values of the Coefficients a_0 and a_1 according to Eq. (4.2) below the Transition Temperature (T_C= 247 K) of Im-ClO_4

Crystal	$M_{2,max}$	a_0	a_1
$ImClO_4$	7.50 G	0.76	0.27

Figure **3** for comparison. Above T_C, on the other hand, the observed M_2 [14] decreases very rapidly as the temperature increases due to the infrequent reorientation of the cation between the non-equivalent potential wells. So that, the observed [14] M_2 was taken to associate with the disorder parameter ($1-P^2$) above T_C for Im-ClO_4.

The temperature dependence of the spin-lattice relaxation time was then calculated from the PS (Eq 2.5) and EF (Eq 2.7) models below and above T_C for Im-ClO_4, as given in Figure **2**. Our results indicate that the inverse spin-lattice relaxation time increases very slightly as the temperature increases below the transition temperature of T_C= 247 K. At the transition temperature T_C, it increases anomalously and reaches its maximum value. Above T_C, it decreases very rapidly up to the 300 K and it is almost constant above 300 K. Although both models (PS and EF) were in good agreement with the observed data [14], the PS model seems to describe it better than the EF model (Figure **2**) with the fitting parameters of Eq. (3.1) as given in Table **1**. These calculated values of the spin-lattice relaxation time from both models were then used to deduce the activation energy U according to Eq. (3.2) as given in Figure **3**. A significant deviation of $ln\,\Gamma$ from linearity above the transition temperature of 247 K (Figure **3**), occurs starting from about 320 K (10^4/T= 31.25 K^{-1}). A similar deviation is observed at about 320

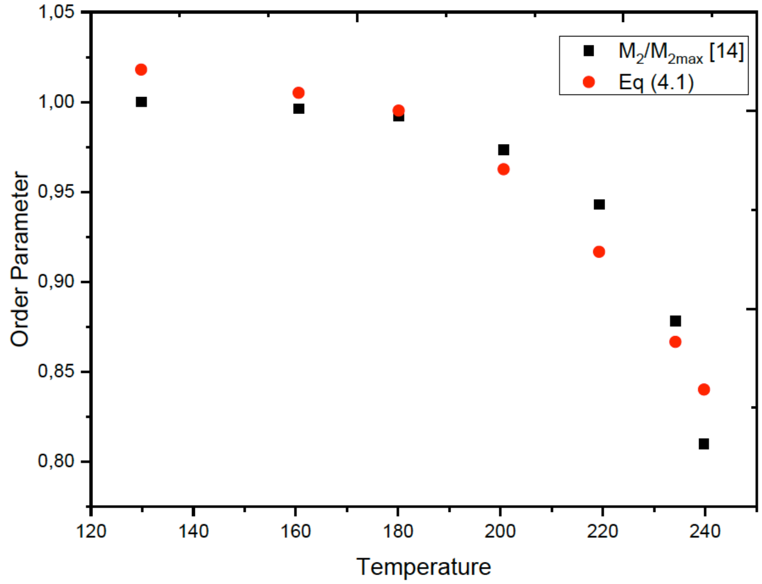

Figure 4: The order parameter ($M_2/M_{2,max}$ [14] and P (Eq. 4.1)) versus temperature below the phase transition temperature of T_C = 247 K in $ImClO_4$.

K in the unit cell volume of Im-ClO_4, so that this illustrates the pretransition effects well pronounced in the DSC experiments, as pointed out previously [14]. Our extracted values of U from the PS model 2.4 and 13.5kJ/mol (Table **2**) below and above T_C, respectively, are very close to those reported [14] values of 3.0 and 16.0 kJ/mol.

5. CONCLUSIONS

The phase transition mechanism in Im-ClO_4 was investigated by calculating the relaxation time and the activation energy of this crystal close to the phase transition at the lower temperature T_C (247 K). The calculated values of the relaxation time from the pseudospin-phonon (PS) and the energy fluctuation (EF) models fit the observed data well. The PS and EF models can be used to predict the mechanism of phase transition for some other molecular ferroelectrics.

REFERENCES

[1] Anderson EB, Long TE. Imidazole- and imidazolium-containing polymers for biology and material science applications. Polymer 2010; 51(12): 2447-2454. https://doi.org/10.1016/j.polymer.2010.02.006

[2] Riduan SN, Zhang Y. Imidazolium salts and their polymeric materials for biological applications. Chem Soc Rev 2013; 42(23): 9055. https://doi.org/10.1039/c3cs60169b

[3] Zhao L, Zhang C, Zhuo L, Zhang Y, Ying JY. Imidazolium Salts: A Mild Reducing and Antioxidative Reagent. J Am Chem Soc 2008; 130(38): 12586-12587. https://doi.org/10.1021/ja8037883

[4] Hanke CG, Price SL, Lynden-Bell RM. Intermolecular potentials for simulations of liquid imidazolium salts. Molec Phys 2001; 99(10): 801-809. https://doi.org/10.1080/00268970010018981

[5] Zhang Y, Chan JYG. Sustainable chemistry: imidazolium salts in biomass conversion and CO_2 fixation. Energy Environ Sci 2010; 3(4): 408-417. https://doi.org/10.1039/B914206A

[6] Lee S. Functionalized imidazolium salts for task-specific ionic liquids and their applications. Chem Commun 2006; 37(31): 1049-1063. https://doi.org/10.1039/b514140k

[7] Seoud OAE, Koschella A, Fidale LC, Dorn S, Heinze T. Applications of ionic liquids in carbohydrate chemistry: A window of opportunities. Biomacromolecules 2007; 8(9): 2629-2647. https://doi.org/10.1021/bm070062i

[8] Yu B, Zhou F, Hu H, Wang C, Liu W. Synthesis and properties of polymer brushes bearing ionic liquid moieties. Electrochim Acta 2007; 53(2): 487-494. https://doi.org/10.1016/j.electacta.2007.07.018

[9] Ma H, Gao W, Wang J, Wu T, Yuan G, Liu J, *et al.* Ferroelectric polarization switching dynamics and domain growth of triglycine sulfate and imidazolium perchlorate. Adv Electron Mater 2016; 2: 1600038. https://doi.org/10.1002/aelm.201600038

[10] Gao W, Chang L, Ma H, You L, Yin J, Liu J, *et al.* Flexible organic ferroelectric films with a large piezoelectric response. NPG Asia Mater 2015; 7(6): e189. https://doi.org/10.1038/am.2015.54

[11] Hu Y, Guo Z, Ragonese A, Zhu T, Khuje S, Li C, *et al.* A 3D-printed molecular ferroelectric metamaterial. PNAS 2020; 117(44): 27204-27210. https://doi.org/10.1073/pnas.2013934117

[12] Zhang Y, Liu Y, Ye HY, Fu DW, Gao W, Ma H, *et al.* A molecular ferroelectric thin film of imidazolium perchlorate that shows superior electromechanical coupling. Angew Chem Int Ed 2014; 126: 5164-5168. https://doi.org/10.1002/ange.201400348

[13] Zhu X, Du M, Feng J, Wang H, Xu Z, Wang L, *et al.* High-Efficiency perovskite solar cells with imidazolium- based ionic liquid for surface passivation and charge transport. Angew Chem Int Ed 2021; 60: 4238-4244. https://doi.org/10.1002/anie.202010987

[14] Pająk Z, Czarnecki P, Szafrańska B, Małuszyńska H, Fojud Z. Ferroelectric ordering in imidazolium perchlorate. J Chem Phys 2006; 124(14): 144502. https://doi.org/10.1063/1.2185098

[15] Czapla Z, Dacko S, Kosturek B, Waskowska A. Dielectric and optical properties related to phase transitions in an imidazolium perchlorate [$C_3N_2H_5ClO_4$] crystal. Phys Stat Sol B 2005; 242: 122-124. https://doi.org/10.1002/pssb.200541249

[16] Przesławski J, Czapla Z. Calorimetric studies of phase transitions in imidazolium perchlorate crystal. J Phys Cond Mat 2006; 18(23): 5517-5524. https://doi.org/10.1088/0953-8984/18/23/021

[17] Kiraci A, Yurtseven H. Damping constant and the relaxation time calculated for the lowest-frequency soft mode in the ferroelectric phase of $Cd_2Nb_2O_7$. Optik 2016; 127: 11497-11504. https://doi.org/10.1016/j.ijleo.2016.09.023

[18] Kiraci A, Yurtseven H. Temperature dependence of the Raman frequency, damping constant and the activation energy of a soft-optic mode in ferroelectric barium titanate. Ferroelectrics 2012; 432:14-21. https://doi.org/10.1080/00150193.2012.707592

[19] Yurtseven H, Kiraci A. Calculation of the damping constant and the relaxation time for the soft-optic and acoustic mode in hexagonal barium titanate. Ferroelectrics 2012; 437: 137-148. https://doi.org/10.1080/00150193.2012.742343

[20] Kiraci A, Yurtseven H. Calculation of the Raman frequency, damping constant (linewidth) and the relaxation time near the tetragonal-cubic transition in $PbTiO_3$. Optik 2017; 14231: 1-319. https://doi.org/10.1016/j.ijleo.2017.06.011

[21] Karacali H, Kiraci A, Yurtseven H. Calculation of the Raman frequency and the damping constant of a coupled mode in the ferroelectric and paraelectric phases in KH_2PO_4. Phys. Stat Sol B 2010; 247: 927-936. https://doi.org/10.1002/pssb.200945181

[22] Yurtseven H, Kiraci A. Damping constant (linewidth) and the relaxation time of the Brillouin LA mode for the ferroelectric-paraelectric transition in $PbZr_{1-x}Ti_xO_3$. IEEE Trans Ultrason Ferroelectr Freq Control 2016; 63: 1647-1655. https://doi.org/10.1109/TUFFC.2016.2572044

[23] Yurtseven H, Kiraci A. Temperature dependence of the damping constant and the relaxation time close to the tetragonal-cubic phase transition in $SrZrO_3$. J Mol Struct 2017; 1128: 51-56. https://doi.org/10.1016/j.molstruc.2016.08.050

[24] Yurtseven H, Kiraci A. Damping constant and the inverse relaxation time calculated as a function of pressure using the X-ray diffraction data close to the cubic-tetragonal phase transition in $SrTiO_3$. Ferroelectrics 2019; 551: 143-151. https://doi.org/10.1080/00150193.2019.1658041

[25] Kiraci A, Yurtseven H. Analysis of the integrated intensity of the central peaks calculated as a function of temperature in the ferroelectric phase of lithium tantalite. Therm Sci 2018; 22(1): 221-227. https://doi.org/10.2298/TSCI170614289K

[26] Laulicht I, Luknar N. Internal-mode line-broadening by proton jumps in KH_2PO_4. Chem Phys Lett 1977; 47(2): 237-240. https://doi.org/10.1016/0009-2614(77)80008-0

[27] Laulicht I. On the drastic temperature broadening of hard mode Raman lines of ferroelectric KDP type crystals near T_C. J. Phys Chem Sol 1978; 39(8): 901-906. https://doi.org/10.1016/0022-3697(78)90153-1

[28] Lahajnar G, Blinc R, Zumer S. Proton spin-lattice relaxation by critical polarization fluctuations in KH_2PO_4. Phys Condens Matter 1974; 18(4): 301-316. https://doi.org/10.1007/BF01464399

[29] Schaack G, Winterfeldt V. Temperature behavior of optical phonons near T_C in triglycine sulphate and triglycine selenite. Ferroelectrics 1977; 15(1): 35-41. https://doi.org/10.1080/00150197708236718

[30] Bartoli FJ, Litovitz TA. Raman scattering: Orientational motions in liquids. J Chem Phys 1972; 56(1): 413-425. https://doi.org/10.1063/1.1676883

[31] Pajak Z, Czarnecki P, Wasicki J, Nawrocik W. Ferroelectric properties of pyridinium periodate. J Chem Phys 1998; 109: 6420-6423. https://doi.org/10.1063/1.477286

[32] Pajak Z, Czarnecki P, Małuszynska H, Szafranska B. Ferroelectric properties of pyridinium fluorosulfonate. J Chem. Phys 2000; 113: 848-853. https://doi.org/10.1063/1.481860